Modelling of BESS/PV Interfaced System Fed BLDC Drive for Electric Vehicle Traction System

K. Sumanth
P.G Student
Department of Electrical & Electronics Engineering
AITAM Engineering College, Andhra Pradesh, India

P. Guruvula Naidu
Senior Assistant Professor
Department of Electrical & Electronics Engineering
AITAM Engineering College, Andhra Pradesh, India

B. Srinivasa Rao
Professor
Department of Electrical & Electronics Engineering
AITAM Engineering College, Andhra Pradesh, India

Abstract

Renewable Energy Sources (RES) such as PV modules, fuel cells deliver output voltage with a high voltage gain converter is essential for the following reasons, such as to maintain high step up voltage, with good output voltage profile with respect to sudden changes in BLDC motor drive. This paper presents the high performance of fast charger for a lithium-ion electric vehicle propulsion battery with PV source. The device is intended to operate in a battery switch station, allowing an up-to 1-h recharge of a 25-kWh depleted battery, removed from a vehicle. The charger is designed as a dual-stage-controlled ac/dc converter. The input stage consists of a three-phase full-bridge diode bridge rectifier combined with a reduced rating of shunt active power filter. The input stage creates an uncontrolled pulsating dc bus while complying with the grid codes by regulating the total harmonic distortion and power factor according to the predetermined permissible limits. The output stage is formed by six interleaved groups of two parallel dc-dc converters, fed by the uncontrolled dc bus with BLDC drive and performing the battery charging process. The charger is capable of operating in any of the three typical charging modes: constant current, constant voltage, and constant power. Extended simulations are shown to demonstrate the functionality of the device.

Keywords: Active Power Filter, BLDC, Multilevel Inverter, DC-DC converter

---

I. INTRODUCTION

Numerous industrial applications have begun to require higher power apparatus in recent years [1].Power-electronic converters are becoming popular for various industrial drives applications. Electrification of the transportation industry is essential due to the improvements in higher fuel economy, better performance, and lower emissions [1]–[4]. In vehicular applications, power electronic dc/dc converters require high power flow capability with wide input range since the terminal voltage of energy storage devices varies with the state of charge (SoC) and load variations. In the case of a electric vehicle (EV), a dc/dc converter interfaces the energy storage device with the motor drive of the traction machine; i.e., the converter is placed between the battery and the high-voltage dc bus.

Numerous advantages of a BLDC motor over a brushed DC motor is absence of the mechanical commutators which allows higher speeds. Brush performance also limits the transient response in case of DC motor. Source of heating in the BLDC motor is the stator, while in the DC motor it is the rotor, therefore it is easier to dissipate heat in the BLDC and reduce audible and electromagnetic noise. Having individual converters has advantages like more flexible individual control and simpler design but does not encourage functionality merging. The power-electronic technology plays a vital role in distributed generation and in integration of renewable energy sources into the electrical grid, and it is widely used and rapidly expanding as these applications become more integrated with the grid-based systems. The increasing number of renewable energy sources and distributed generators requires new strategies for the operation and management of the electricity grid in order to maintain or even to improve the power-supply reliability and quality. There are two common types of vehicle battery chargers. The onboard (often referred to as slow or low power) charger is located on board. The propulsion battery is recharged via the slow charger, plugged into a charging spot, while the vehicle is at parking lot [7]–[14]. The off board (so-called fast or high power) charger is located at the battery switch station (BSS). The battery must be removed from the vehicle to be recharged via the fast charger (FC) as well as replaced to renewable energy source has been used PV cell with respective high voltage gain converter.

Apart from non-linear loads, events like capacitor switching, motor starting and unusual faults could also inflict power quality (PQ) problems. PQ problem is defined as any manifested problem in voltage/current or leading to frequency deviations that result in failure or mal-operation of customer equipment. Alternatively, a more elegant approach employs a shunt-connected active power filter (APF) at the uncontrolled rectifier input, supplying the reactive current to the diode rectifier, thus achieving both near-unity PF and near-zero total harmonic distortion (THD) by letting the utility to supply the active current only, which is

in phase with the utility voltage and of the same shape. PQ compensators can be categorized into two main types. One is shunt connected compensation device that effectively eliminates harmonics. The other is the series connected device, which has an edge over the shunt type for correcting the distorted system side voltages and voltage sags caused by power transmission system faults [1], these power quality problems may cause abnormal operations of facilities or even trip protection devices. Hence, the maintenance and improvement of electric power quality has become an important scenario today.

This paper describes the development of a 50-kW commercial FC, employed in the first generation of BSS in Israel. Rather than presenting a novel topology, the main goal of this paper is to present a successful industrial application of well-known power electronics concepts. The charger employs a three-phase diode rectifier combined with three single-phase APFs as the input stage and twelve buck dc–dc converters, separated into six interleaved groups as the output stage. The power stage of the charger operates as a programmable voltage supply with controllable dynamic current limitation.

II. FC REQUIREMENTS

The FC, described in this paper, was designed to charge 355-V 70-A traction batteries formed by 96S2P connection of 3.7-V 35-A h lithium manganese spinal cells.

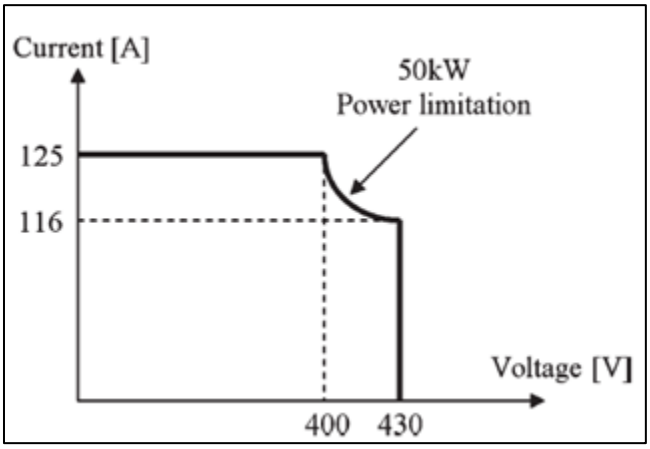

Fig. 1: FC output performance envelope.

A. At Output Stage:

In order to charge such a battery, the FC must be able to operate in the full range of the possible battery voltages. In addition, power cable voltage drop should be taken into account. Hence, the maximum output voltage design requirement was set to 430 V. The maximum charging current was limited by the battery manufacturer to 125 A for safety reasons, leading to the charger output performance envelope requirement, shown in Fig. 1.

B. Input Stage:

The charger was designed to draw the power from 380- to 415-Vrms 50-Hz three-phase grids with neutral and protective earth connections. Since typical grid operators provide the ac power with 10% accuracy, the charger must be capable of functioning in the range of 342–457-Vrms input line voltages. The minimum consumer PF allowed by the Israel Electric Company in Israel is 0.92. Note that devices with active power correction usually operate with near-unity displacement factor (DF); therefore, the PF is affected mostly by the THD according to the following well-known relation:

$$PF = \frac{DF}{\sqrt{1+THD^2}}$$

In case the DF is kept near unity, the theoretical maximum allowed value of THD is 42.6%. However, since the rated input current exceeds 16 A, the charger emissions must comply with the IEC61000-3-4 standard, leading to the THD upper limit of 15%.

III. PROPOSED SYSTEM

The system-level block diagram of the proposed solution is presented in Fig. 2. On the signal level, the FC communicates with traction battery management system (BMS) and CMS terminal via CAN and Ethernet buses, respectively. The charger supports both master and slave mode charging. In the master mode, the charger performs either CC–CV of CP charging according to the CMS commands while monitoring the battery condition. In the slave mode, the battery manages the charging process by sending current/voltage/power requests to the charger. The CMS is the highest level management layer of a BSS, performing

administration and billing tasks in addition to the ability of limiting or completely shutting down the FC fleet power in case of a safety issue or according to the utility grid operator request. In the charger under study, both communication protocols are realized by Zilog eZ80F91 microcontroller with the assistance of Grid connect RS232-CAN adaptor since eZ80F91 does not support the CAN bus directly. Zilog microcontroller is a bidirectional gateway between the CMS, battery BMS, and the Atmel At mega 128 microcontroller, which is in charge for the power management and monitoring of the charger power circuitry. The APF and buck control boards are independent and based on fully analog controllers. On the power level, there are low- and high-voltage links between the charger and the battery. The high-voltage link transfers the charging power, while the low-voltage (12 V) low-power link supplies power to the battery contactors. Note that the 12-V power supply, located inside the FC, is used to power both charger and battery contactors. The battery contactors are used to isolate the high-voltage power pack from the environment when the battery is not located in the vehicle or charging.

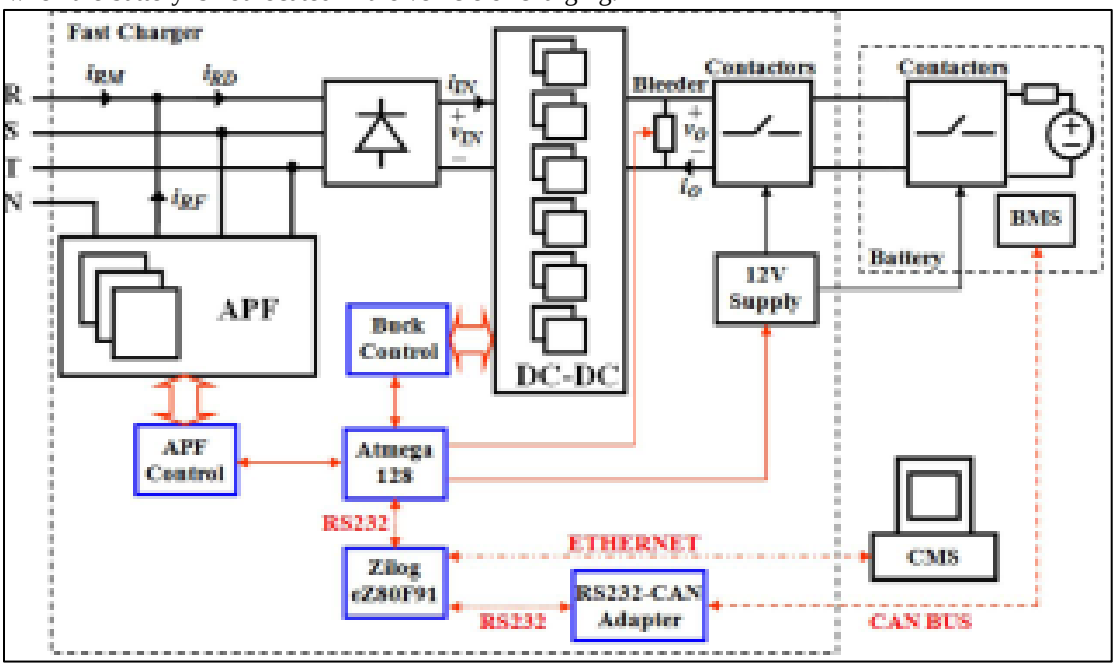

Fig. 2: FC system-level block diagram

Additional feature of the battery contactors is pre-charging of the vehicle inverter dc link capacitor upon battery connection. The charger contactors serve similar purposes since the charger dc–dc stage contains output capacitors which must be carefully pre-charged prior to the battery connection in order to prevent excessive inrush currents.

When a charging process is terminated, the charger output voltage is usually higher than 400 V. After the battery is disconnected, the output capacitors should be discharged to a low voltage because of safety reasons. This is accomplished by a bleeder circuit, discharging the output capacitors quickly below 50 V. The bleeder and the 12-V contactor power supply are both operated by the Atmega 128 microcontroller.

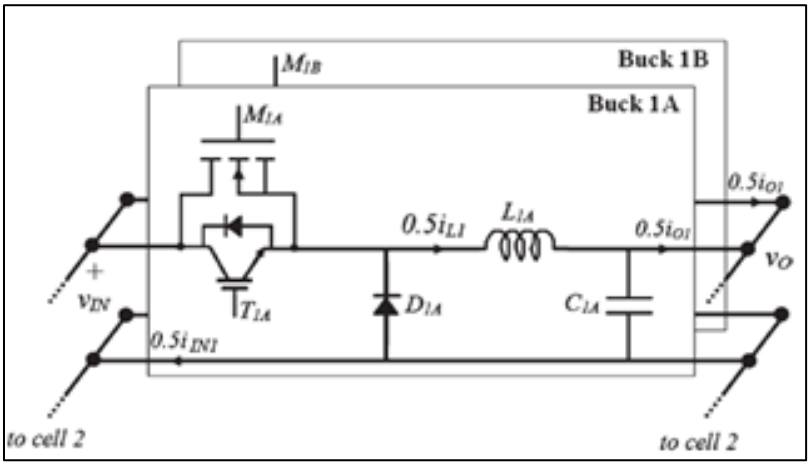

Fig. 3: Buck cell structure.

The dc–dc stage of the charger consists of six interleaved cells of two parallel 4.5-kVA buck converters [47], [48]. A single cell structure is shown in Fig. 3. The converters are of basic buck topology with an enhanced switch, consisting of a parallel

connection of insulated gate bipolar transistor (IGBT) and MOSFET. A small delay between the turn-on and turnoff instants of the transistors allows relatively high switching frequency operation of 50 kHz and significant loss reduction. Detailed operation of the combined switch is out of the current paper scope and will be reported in a separate paper. The pulsewidth-modulation (PWM) signals of the two converters in the same cell are synchronized while the PWM signals of the two adjacent cells are 60◦ shifted in order to implement time-based interleaving. While the ripple of cell output current *ion* is around 6 A ($n = 1 \ldots 6$), the FC output current ripple is reduced to 0.7 A as a result of interleaving. In addition, the ripple frequency is multiplied by six, and as a result, its influence on the battery current further reduces because of the low-pass characteristics of the battery internal impedance [49]. The dc–dc stage input current ripple is much improved as well, leading to the electromagnetic emission reduction as follows. Since basic buck topology is used, the input cell current is highly discontinuous, dropping to zero each time the switch is open. However, due to interleaving, the input current ripple is significantly reduced, and its frequency is multiplied by six as well. The input current of the dc–dc stage loads the diode bridge; hence, the current ripple is polluting the mains since the APF stage is unable to suppress high-frequency harmonics. Both ripple reduction and frequency increase lead to THD reduction and electromagnetic compatibility filter requirements loosening. The voltage at the input of the dc–dc stage is the rectified input voltage (for 400-V_{rms} grid). Since buck topology is employed at the output stage, the minimum value of the rectified voltage must be higher than the maximum output dc voltage in order to ensure undistorted operation. The minimum value of the rectified voltage is given by

$$V_{IN\,\min} = \frac{\sqrt{6}}{2} V_{rms}$$

Hence, the global minimum of the rectified voltage (neglecting the voltage drop of the diode bridge) is *VINmin* = 419 V for *V*rms = 342 V, and the requirement of maximum charge output voltage of 430 V cannot be met. As a result, the modification of the maximum output voltage requirement shown in Fig. 4 was proposed and accepted by the customer. It is worth noting that 410-V output is sufficient to charge the mentioned battery in most cases if the power cable is of a reasonable length and cross-sectional area since, during CV and CP charging stages, the current diminishes and cable voltage drop reduces proportionally with the current.

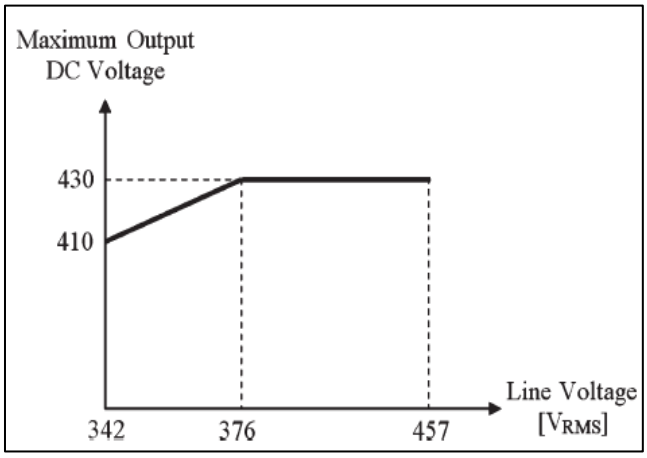

Fig. 4: Modified maximum output voltage envelope.

The architecture of the dc–dc stage control circuitry is shown in Fig. 5. The analog control board receives from the Atmega 128 microcontroller reference voltage command in case of CV operation or reference current command in case of CC or CP operation, senses the real values of the appropriate voltage/ current, and creates PWM commands to switch drivers. The control algorithm has a conventional dual-loop structure, where the slow outer loop controls the charger output parameter (voltage or current, according to the operation mode) and the inner current mode control (CMC) loop controls the inductor currents of the individual converters to follow the outer loop generated reference. The interleaving is achieved by shifting the clocks used by CMC. The PWM signal, created by the current loop, is split into two time-delayed signals to the drivers of the combined switch transistors. Actual currents, voltages, and cell temperatures are continuously monitored by the Atmega 128 microcontroller, which can shut cells down in case of malfunction and perform corresponding output power derating. Control loop design and component selection issues are omitted for the sake of brevity.

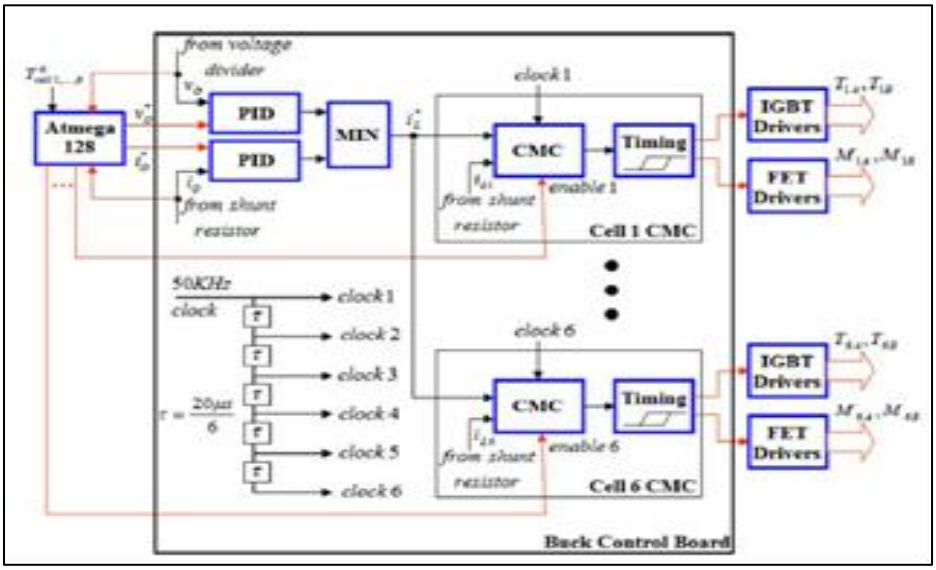

Fig. 5: DC–DC stage control circuitry diagram.

The FC input stage consists of a three-phase diode rectifier and three single-phase APFs [50]. The reason of using three single-phase APFs instead of a single three-phase APF is the fact that a single-phase APF module was developed earlier by the company for another application and was found suitable for the first version of the FC. A three-phase APF employment is currently being developed for the future versions of the device. The diagram of the input stage phase *R* is shown in Fig. 6. The diode bridge is represented by a nonlinear current source i_{RD}, which is supplied by both the mains and the APF. The main idea is forcing the APF to supply the reactive and harmonic content of the nonlinear current, leaving the mains to supply the fundamental harmonic only. The APF consists of a controlled full bridge with a dc bus capacitor (since it does not provide real power to the diode bridge), connected to the ac bus via an inductor. Although the diode bridge is represented by a current source, its actual behavior resembles a CP load since it drives a battery through dc–dc converter stage.

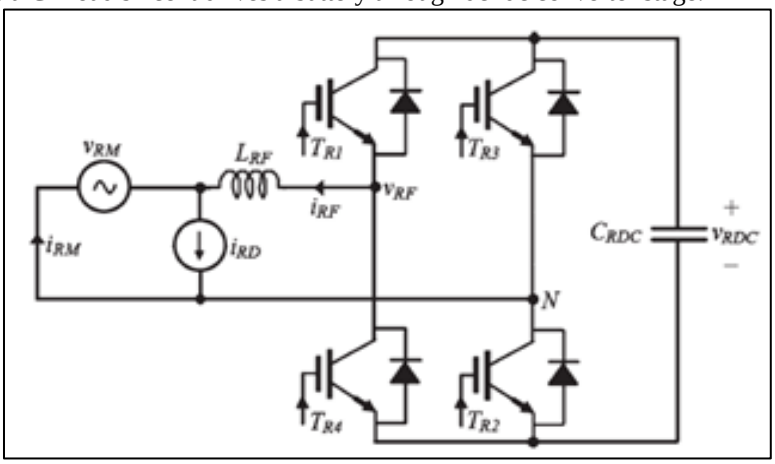

Fig. 6: Input stage R-phase diagram.

In order to realize, the dc link voltage of the APF should be kept above the absolute maximum of the mains voltage because of the buck structure of the circuit. In addition, since there are internal switching and conduction losses in the APF, some amount of active current should be drawn by the filter from the mains to maintain the dc link voltage nearly constant. Moreover, there is a following trade-off between the dc link voltage level and filter inductor: In order to prevent the switching frequency leakage, the inductor value should be as high as possible; however, a high inductor leads to the high frequency harmonics compensating ability deterioration since the dc link voltage increase is limited by the capacitor voltage rating. The trade-off values are eventually determined by PF and THD design requirements. If no solution is available satisfying all the constraints, an *LC* filter instead of a single inductor may be considered. However, in this case study, a single inductor solution turned out to be sufficient.

IV. MATLAB MODELING AND SIMULATION RESULTS

Here simulation is carried out in two different conditions, in that 1.Proposed Battery Charger with DC-DC Converter with Power Factor Correction Scheme. 2. Proposed Battery Charger with DC-DC Converter with PV Source with BLDC drive.

A. Case 1: Proposed Battery Charger with DC-DC Converter with Power Factor Correction Scheme.

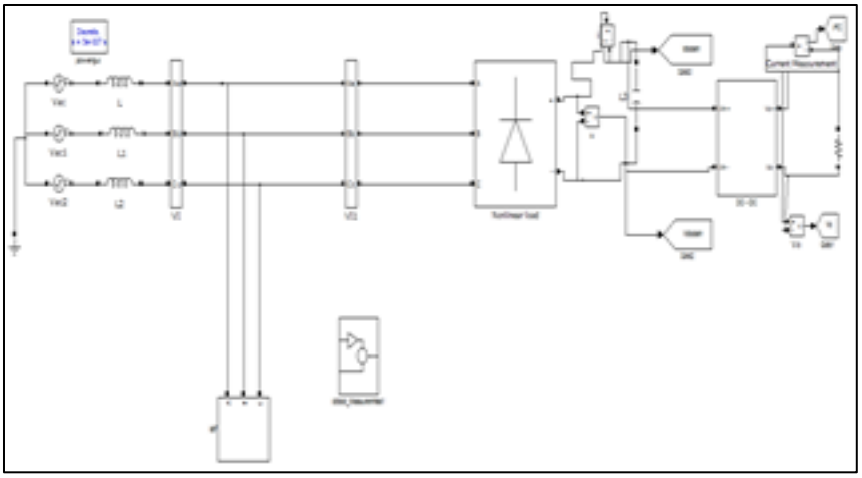

Fig. 7: Matlab/Simulink Model of Proposed Battery charger with DC-DC Converter

Fig.7 shows the Matlab/Simulink Model of Proposed Battery charger with DC-DC Converter using Matlab/Simulink Software package.

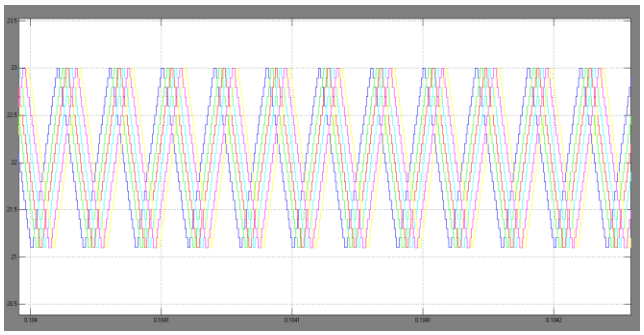

Fig. 8: Individual buck cell inductor currents

Fig.8 shows the Individual buck cell inductor currents of Proposed Battery charger with DC-DC Converter.

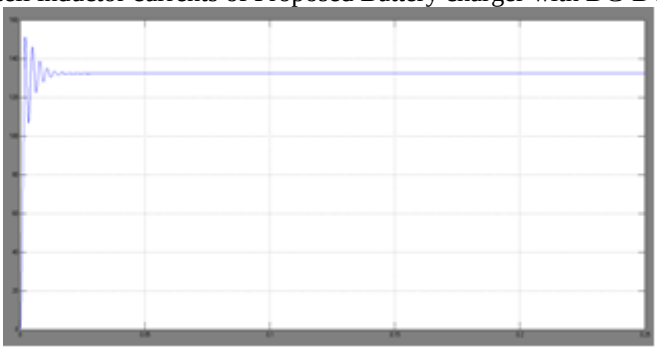

Fig. 9: FC output current after capacitor filter

Fig.9 shows the FC output current after capacitor filter of Proposed Battery charger with DC-DC Converter.

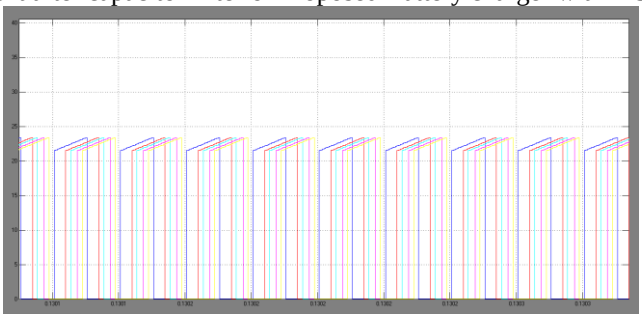

Fig. 10: Individual buck cell improved input currents

Fig.10 Individual buck cell Improved input currents of Proposed Battery charger with DC-DC Converter.

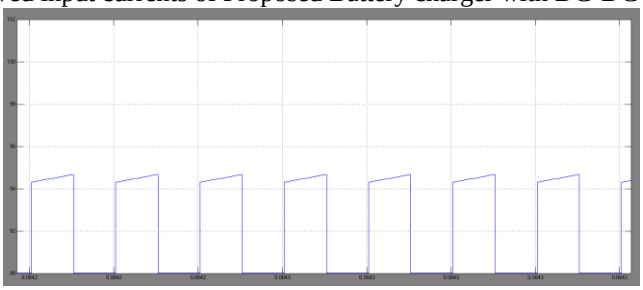

Fig. 11: DC–DC stage input current

Fig.11 shows the DC–DC stage improved input current of Proposed Battery charger with DC-DC Converter.

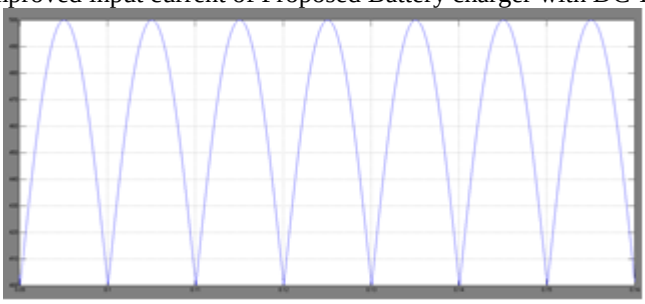

Fig. 12: Rectified voltage at the dc–dc stage input

Fig.12 shows the Rectified voltage at the dc–dc stage input of Proposed Battery charger with DC-DC Converter.

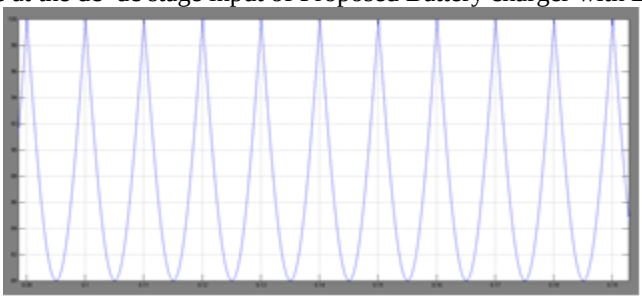

Fig. 13: Worst case bridge rectifier output current

Fig.13 shows the Worst case bridge rectifier output current of Proposed Battery charger with DC-DC Converter.

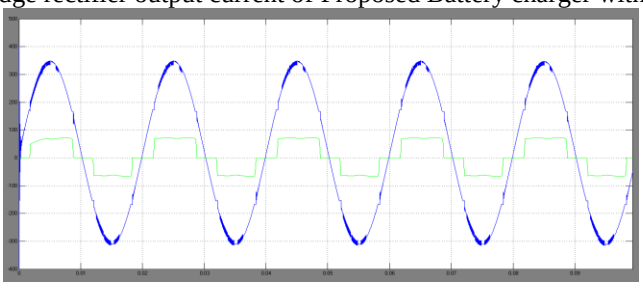

Fig. 14: Input stage *R*-phase mains voltage and Diode Bridge current

Fig.14 shows the Input stage *R*-phase mains voltage and Diode Bridge current.

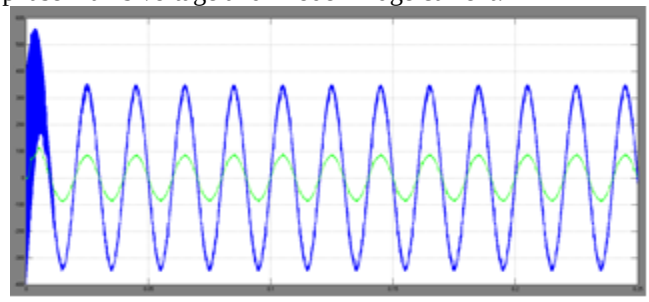

Fig. 15: Supply Voltage & Current

Fig.15 shows the Supply Voltage & Current of Proposed Battery charger with DC-DC Converter.

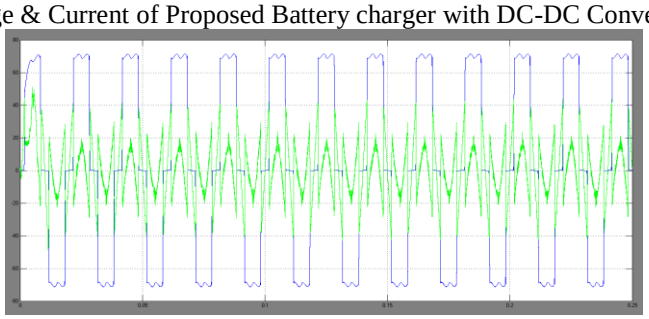

Fig. 16: Load Currents & Compensation Current

Fig.16 Load Currents & Compensation Current of Proposed Battery charger with DC-DC Converter.

B. Case 2: Proposed Battery Charger with DC-DC Converter with PV Source with BLDC Drive:

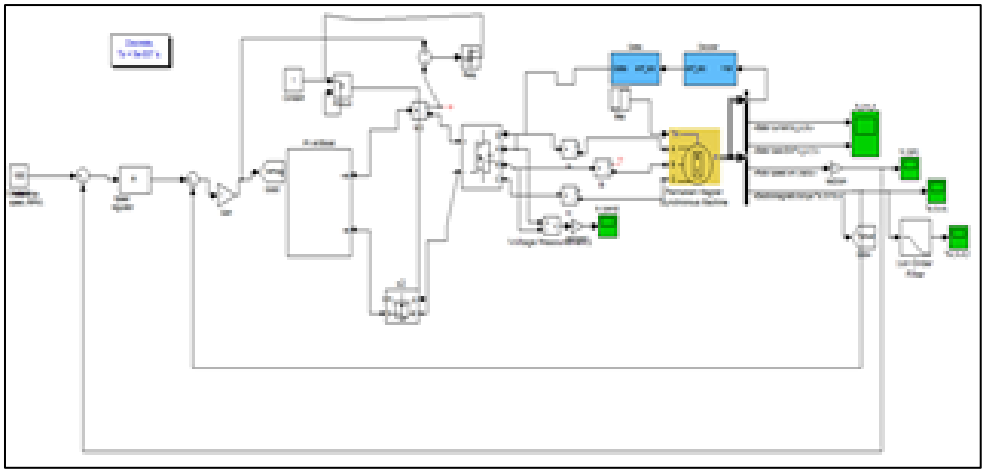

Fig. 17: Matlab/Simulink Model of Proposed Battery charger with DC-DC Converter with PV Source with BLDC Drive

Fig.17 shows the Matlab/Simulink Model of Proposed Battery charger with DC-DC Converter with PV Source with BLDC drive using Matlab/Simulink Software package.

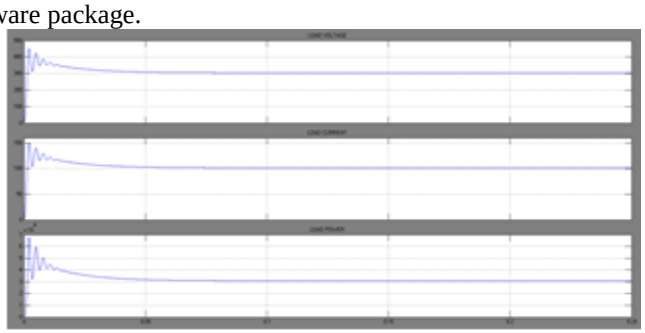

Fig. 18: Load Voltage, Load Current, Load Power

Fig.18 shows the Load Voltage, Load Current, and Load Power of Proposed Battery Charger with DC-DC Converter with PV Source under BLDC Drive system, due to maintain constant load condition as well as achieve the load with high stability.

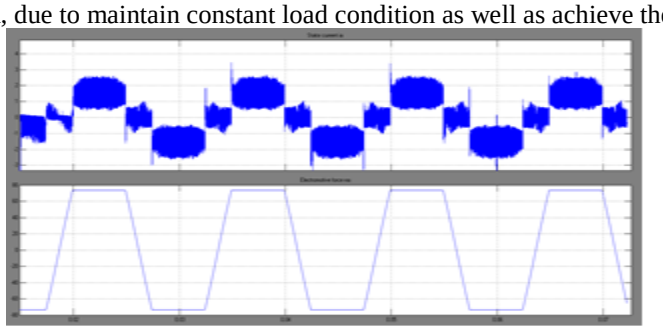

Fig. 19: Stator Current & Back EMF

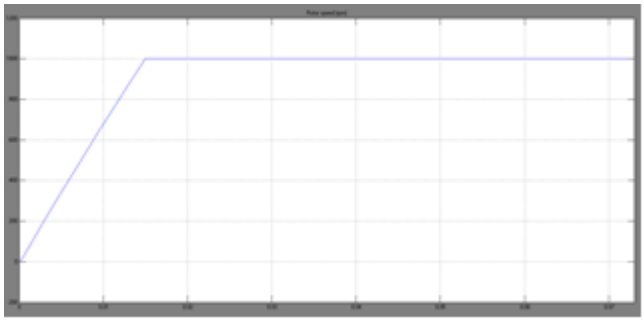

Fig. 20: Speed

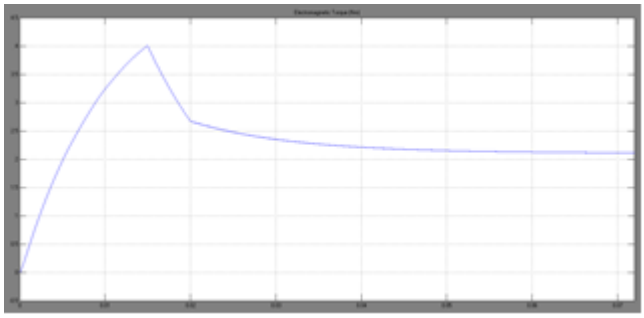

Fig. 21: Electromagnetic Torque

V. CONCLUSION

BLDC have been used in different applications such as industrial automation, automotive, aerospace instrumentation and appliances since 1970's. This paper has proposed Single phase and Three Phase power conversion system with BLDC drive application. A number of integrated energy systems based on a compact converter topology. The device is capable of supplying up to 50-kW charging power to any battery, operating in 240–430-V voltage range in CC, voltage, or power mode. The charger topology may be referred to as a two stage controlled rectifier. The input stage consists of a three phase full-bridge rectifier combined with a reduced rating APF (three single-stage power filters are actually employed). The input stage creates an uncontrolled dc bus while complying with the grid codes by keeping the THD and PF within the permissible limits. The output stage is formed by six interleaved groups of two dc–dc converters, reducing the input and output current ripples. Two independent control boards are employed: active filters control circuitry and the dc–dc control circuitry. The designed device performance is shown to comply with main design requirements, and simulation results are presented.

REFERENCES

[1] B. Kennedy, D. Patterson, and S. Camilleri, "Use of lithium-ion batteries in electric vehicles," J. Power Sources, vol. 90, no. 2, pp. 156–162, Oct. 2000.
[2] R. Gitzendanner, F. Puglia, C. Martin, D. Carmen, E. Jones, and S. Eaves, "High power and high energy lithium-ion batteries for underwater vehicles," J. Power Sources, vol. 136, no. 2, pp. 416–418, Oct. 2004.
[3] G.-C. Hsieh, L.-R. Chen, and K.-S. Huang, "Fuzzy controlled Li-ion battery charge system with active state-of-charge controller," IEEE Trans. Ind. Electron., vol. 48, no. 3, pp. 585–593, Jun. 2001.
[4] M. Chen and G. Rincon-Mora, "Accurate, compact, and power-efficient Li-ion battery charger circuit," IEEE Trans. Circuits Syst. II, Exp. Briefs, vol. 53, no. 11, pp. 1180–1184, Nov. 2006.
[5] K. Tsang and W. Chan, "A simple and low-cost charger for lithium-ion batteries," J. Power Sources, vol. 191, no. 2, pp. 633–635, Jun. 2009.
[6] J.-J. Chen, F.-C. Yang, C.-C. Lai, Y.-S. Hwang, and R.-G. Lee, "A high efficiency multimode Li-ion battery charger with variable current source and controlling previous stage supply voltage," IEEE Trans. Ind. Electron.,vol. 56, no. 7, pp. 2469–2478, Jul. 2009.
[7] D. Thimmesch, "An SCR inverter with an integral battery charger for electric vehicles," IEEE Trans. Ind. Appl., vol. IA-21, no. 4, pp. 1023– 1029, Jul. 1985.
[8] J. Bendien, G. Fregien, and J. vanWyk, "High-efficiency on-board battery charger with transformer isolation, sinusoidal input current and maximum power factor," Proc. Inst. Elect. Eng.—Elect. Power Appl., vol. 133, no. 4, pp. 197–204, Jul. 1986.
[9] S.-K. Sul and S.-J. Lee, "An integral battery charger for four-wheel drive electric vehicle," IEEE Trans. Ind. Appl., vol. 31, no. 5, pp. 1096–1099, Sep./Oct. 1995.
[10] B. Masserant and T. Stuart, "A maximum power transfer battery charger for electric vehicles," IEEE Trans. Aerosp. Electron. Syst., vol. 33, no. 3, pp. 930–938, Jul. 1997.
[11] D. Jackson, A. Schultz, S. Leeb, A. Mitwalli, G. Verghese, and S. Shaw, "A multirate digital controller for a 1.5 kW electric vehicle battery charger," IEEE Trans. Power Electron., vol. 12, no. 6, pp. 1000–1006, Nov. 1997.
[12] L. Solero, "Nonconventional on-board charger for electric vehicle propulsion batteries," IEEE Trans. Veh. Technol., vol. 50, no. 1, pp. 144–149, Jan. 2001.
[13] M. Egan, D. O'Sullivan, J. Hayes, M. Willers, and C. Henze, "Powerfactor- corrected single-stage inductive charger for electric vehicle batteries," IEEE Trans. Ind. Electron., vol. 54, no. 2, pp. 1217–1226, Apr. 2007.

[14] G. Pellegrino, E. Armando, and P. Guglielmi, "An integral battery charger with power factor correction for electric scooter," IEEE Trans. Power Electron., vol. 25, no. 3, pp. 751–759, Mar. 2010.
[15] N. Kutkut, D. Divan, D. Novotny, and R. Marion, "Design considerations and topology selection for a 120 kW IGBT converter for EV fast charging," IEEE Trans. Power Electron., vol. 13, no. 1, pp. 169–178, Jan. 1998.
[16] C.-H. Lin, C.-Y. Hsieh, and K.-H. Chen, "A Li-ion battery charger with smooth control circuit and built-in resistance compensator for achieving stable and fast charging," IEEE Trans. Circuits Syst. I, Reg. Papers,vol. 57, no. 2, pp. 506–517, Feb. 2010.
[17] Better Place Inc., The Solution: Switch Stations, 2011. [Online]. Available: http://www.betterplace.com/the-solution-switch-stations
[18] M. Hartmann, T. Friedli, and J.W. Kolar, "Three-phase unity power factor mains interfaces of high power EV battery charging systems," presented at the Proc. ECPE Power Electron. Charging Elect. Veh. Workshop,Valencia, Spain, Mar. 21–22, 2011.
[19] J. Orr, A. Emanuel, and K. Oberg, "Current harmonics generated by a cluster of electric vehicle battery chargers," IEEE Trans. Power App. Syst., vol. PAS-101, no. 3, pp. 691–700, Mar. 1982.
[20] J. Orr, A. Emanuel, and D. Pileggi, "Current harmonics, voltage distortion and powers associated with battery chargers," IEEE Trans. Power App. Syst., vol. PAS-101, no. 8, pp. 2703–2710, Aug. 1982.
[21] J. Orr, A. Emanuel, and D. Pileggi, "Current harmonics, voltage distortion and powers associated with battery chargers distributed on the residential power system," IEEE Trans. Ind. Appl., vol. IA-20, no. 4, pp. 727–734, Jul. 1984.
[22] S. Rahman and G. Shrestha, "An investigation into the impact of electric vehicle load on the electric utility distribution system," IEEE Trans. Power Del., vol. 8, no. 2, pp. 591–597, Apr. 1993.
[23] P. Staats,W. Grady, A. Arapostathis, and R. Thallam, "A statistical method for predicting the net harmonic currents generated by a concentration of electric vehicle battery chargers," IEEE Trans. Power Del., vol. 12, no. 3, pp. 1258–1266, Jul. 1997.